

1 **Controlled chamber formation of per- and polyfluoroalkyl substances** 2 **(PFAS) aerosols with *Pseudomonas fluorescens*: size distributions,** 3 **effects, and inhalation deposition potential**

4 Ivan Kourtchev¹, Steve Coupe¹, Allison Buckley², Jishnu Pandamkulangara Kizhakkethil¹, Elena Gatta³,
5 Dario Massabò^{3,4}, Paolo Prati^{3,4}, Virginia Vernocchi⁴, and Federico Mazzei^{3,4}

6 ¹Centre for Agroecology Water and Resilience (CAWR), Coventry University, Wolston Lane, Ryton on Dunsmore, CV8 3LG,
7 UK

8 ²Toxicology Department, Radiation, Chemical, Climate and Environmental Hazards Directorate, UK Health Security Agency,
9 Harwell Campus, Chilton, Oxfordshire, OX11 0RQ, UK

10 ³Dipartimento di Fisica, Università di Genova, Genoa, Italy

11 ⁴Istituto Nazionale di Fisica Nucleare (INFN), Sezione di Genova, Genoa, Italy

12 *Correspondence to:* Ivan Kourtchev (ivan.kourtchev@coventry.ac.uk)

13 **Abstract.** Per- and polyfluoroalkyl substances (PFAS) are recognised as atmospheric contaminants, yet processes governing
14 their aerosol formation, size distribution, and interactions with atmospheric particle surfaces remain unknown. We investigated
15 aerosolisation and size-resolved behaviour of 25 PFAS covering short-, medium-, and long-chain perfluoroalkyl carboxylic
16 acids (PFCA), perfluoroalkane sulfonates, fluorotelomer sulfonates and emerging alternatives. Experiments were conducted
17 under controlled chamber conditions using a water–organic solvent system, in the absence/presence of the model bacterium
18 *Pseudomonas fluorescens* seed, ~~to investigate the potential influence of microbial presence on PFAS behaviour~~
19 ~~of wastewater-impacted environments~~. Most PFAS exhibited unimodal mass–size distributions peaking at 0.3 µm, indicating
20 dominant association with the fine mode. Sulfonated PFAS showed broadly similar aerosol-phase concentrations regardless
21 of carbon-chain length, whereas PFCA displayed increasing aerosolisation with chain length. Perfluorooctane sulfonic acid
22 (PFOS) showed additional ultrafine enrichment, 6:2 fluorotelomer sulfonate (6:2 FTS) and sodium 4,8-dioxa-3H-
23 perfluorononanoate (NaDONA) exhibited broader size profiles, suggesting compound-specific effects linked to volatility and
24 interfacial behaviour. *Pseudomonas fluorescens* seed did not enhance PFAS aerosol concentrations through condensation or
25 heterogeneous uptake onto bacterial particles or shift in modal diameters, and no enrichment was observed at bacterial size
26 mode, indicating limited PFAS–bioaerosol association under the tested conditions. Multiple-Path Particle Dosimetry (MPPD)
27 modelling based on the measured size distributions predicted substantial deposition of the aerosol-bound PFAS in the
28 pulmonary region, particularly for compounds enriched in ultrafine particles. Our findings indicate that PFAS aerosol
29 behaviour in mixed-solvent systems is controlled primarily by physical droplet generation and evaporation, with implications
30 for airborne transport and inhalation exposure from contaminated aqueous sources.

31 1 Introduction

32 Per- and polyfluoroalkyl substances (PFAS) are synthetic organofluorine compounds widely used in industrial and consumer
33 applications due to their high thermal stability and strong surface-active behaviour (Glüge et al., 2020). Their persistence,
34 mobility, and potential toxicity have raised growing environmental and health concerns, particularly given their ubiquitous
35 presence in water, soil, and the atmosphere (see reviews Evich et al., 2022; Faust, 2023). Atmospheric transport is now
36 recognised as an important pathway for the redistribution of PFAS on regional and global scales (Barber et al., 2007; Ellis et
37 al., 2004; Kourtchev et al., 2024; Kourtchev et al., 2025; Schenker et al., 2008), yet the mechanisms by which these compounds
38 enter and are stabilised in the atmospheric particle phase remain poorly understood.

39 PFAS are surfactants that readily accumulate at air–water interfaces (Schaefer et al., 2019) and adsorb onto mineral (Alves et
40 al., 2020; Folorunsho et al., 2025), organic (Wanzek et al., 2023), and biological surfaces (Dai et al., 2023). Their strong
41 interfacial activity suggests that pre-existing airborne particles could act as carriers or “seeds” for PFAS, facilitating their
42 transfer from aqueous systems into the atmosphere. Laboratory studies with sea-spray aerosol have shown that PFAS
43 enrichment in surface films exceeds that of bulk water by several orders of magnitude (Johansson et al., 2019), supporting the
44 likelihood of interfacial transfer. In the atmosphere, aerosol particles can grow through the condensation of semi-volatile
45 compounds when ambient vapour pressures fall below equilibrium values, leading to vapour uptake by existing particles
46 (Romakkaniemi et al., 2011; Stolzenburg et al., 2018). The rate and extent of condensation depend on compound volatility,
47 surface tension, and relative humidity, as well as particle composition. For surface-active species such as PFAS, adsorption or
48 condensation at particle interfaces may not only contribute to particle growth but also promote their association with pre-
49 existing aerosols, effectively turning these particles into carriers for atmospheric transport. Interactions with organic or
50 biological material may further modify these processes by altering surface energy, hygroscopicity, and the stability of particle-
51 bound PFAS. Wastewater treatment plants (WWTPs) are of particular interest in this context, as they are recognised co-sources
52 of both PFAS (Cookson [and](#) Detwiler, 2022) and biological aerosols, also known as bioaerosol (Li et al., 2016; Poopedi et
53 al., 2025; Xu et al., 2020). During aeration and mechanical agitation, fine droplets containing PFAS and microbial material
54 can become airborne, providing a direct mechanism for PFAS transfer from water to air. Elevated concentrations of PFAS are
55 frequently detected in WWTP effluents and sludges (Cookson [and](#) Detwiler, 2022), and both PFAS and bioaerosol emissions
56 from aeration tanks are well documented (Ahrens et al., 2011; Li et al., 2016; Lin et al., 2022; Pandamkulangara Kizhakkethil
57 et al., 2025; Poopedi et al., 2025; Shoeib et al., 2016; Xu et al., 2020).

58 Despite growing evidence for PFAS volatilisation and enrichment during water-to-air transfer (Ahrens et al., 2011; Lin et al.,
59 2022; Pandamkulangara Kizhakkethil-[& and](#) Kourtchev, 2025; Pandamkulangara Kizhakkethil et al., 2024; Shoeib et al.,
60 2016), the potential involvement of biological aerosol particles in facilitating PFAS aerosolisation remains unexplored.
61 Literature indicates that bioaerosols can participate in heterogeneous chemical processes (e.g., Ervens [&and](#) Amato, 2020;
62 Estillore et al., 2016), suggesting that similar behaviour may occur for PFAS. Recent work has shown that PFAS can associate
63 with bacterial cells, primarily through adsorption to cell surfaces and, to a lesser extent, through limited uptake into cell

64 interiors (Dai et al., 2023). Controlled batch and miscible-displacement studies using *Pseudomonas aeruginosa* (Gram-
65 negative) and *Bacillus subtilis* (Gram-positive) demonstrated substantial retention and increased retardation of perfluorooctane
66 sulfonic acid (PFOS), one of the most studied PFAS, in bacterial-inoculated porous media. While these observations are
67 derived from aqueous and porous-media systems and cannot be directly extrapolated to the atmosphere, they provide a useful
68 conceptual analogue: if bacterial cell surfaces in water promote PFAS association, analogous surface-mediated interactions
69 could, in principle, occur with airborne biological particles. To date, however, no studies have examined PFAS interactions
70 with bioaerosols in the atmospheric context, highlighting a clear and unaddressed research gap. In principle, microbial cells or
71 their fragments could either enhance PFAS partitioning into the particle phase through sorptive or condensation processes or
72 inhibit it via electrostatic or interfacial competition.

73 Understanding whether and how biological matter influences PFAS aerosol behaviour is therefore essential for accurately
74 assessing emission pathways from engineered systems such as including but not limited to WWTPs. WWTPs represent one
75 example of environments in which PFAS and biological aerosols may co-occur, highlighting the broader relevance of
76 understanding PFAS–bioaerosol interactions, rather than serving as a system directly replicated in this study. Furthermore,
77 PFAS–bioaerosol interactions may alter the hygroscopicity and atmospheric lifetime of emitted particles, with implications
78 for transport and deposition.

79 A further uncertainty concerns the atmospheric transport, deposition, and human exposure potential of PFAS, all of which are
80 intrinsically linked to particle size. Particle size governs the residence time and dispersal range of aerosols (Finlayson-Pitts
81 and Pitts, 2000), their efficiency of dry and wet deposition (Farmer et al., 2021) and likelihood of respiratory uptake (Tsuda
82 et al., 2013). Smaller submicron particles (<1 µm) have low gravitational settling velocities and long atmospheric residence
83 times, allowing efficient transport over long distances, whereas coarse particles are more readily removed from the atmosphere
84 near emission sources through sedimentation and impaction (Zhang and Vet, 2006). Particle size also governs deposition
85 behaviour and associated health outcomes: fine and ultrafine particles can penetrate deep into the pulmonary region of
86 respiratory systems and reach the alveoli, where they are linked to cardiovascular and respiratory morbidity (Pope III and
87 Dockery, 2006), whereas coarse particles deposit mainly in the upper airways and have been shown to induce inflammation
88 and allergic responses (Wu et al., 2018).

89 Despite its importance, size-resolved information on PFAS in aerosols remains scarce and not always in agreement (Dreyer et
90 al., 2015; Ge et al., 2017; Guo et al., 2018; Harada et al., 2006; Lin et al., 2022). Some of these studies considered a limited
91 number of PFAS, typically a few legacy compounds such as perfluorooctanoic acid (PFOA) and PFOS or employed samplers
92 with only a few size fractions (e.g. n=5), which makes direct comparison with other studies difficult.

93 Reported aerosol size distributions vary with compound class, particle size range, and sampling context. In a semi-rural setting
94 in Germany, Dreyer et al. (2015) observed PFOA predominantly associated with ultrafine and submicron particles (< 0.14
95 µm), whereas PFOS showed enrichment in the supermicron range (1.4–3.8 µm). Ge et al. (2017) reported ionic PFCAs mainly
96 associated with fine particles (< 0.5 µm) in indoor environments, while PFOS was enriched in coarse roadside aerosols (2.5–
97 10 µm). In contrast, Guo et al. (2018) observed bimodal size distributions in urban aerosols during haze conditions, with PFOA

98 [present in both fine \(0.4–2.1 \$\mu\text{m}\$ \) and coarse \(3.3–10 \$\mu\text{m}\$ \) modes and PFOS largely associated with coarse particles. Lin et al.](#)
99 [\(2022\) further observed compound-specific aerosol mass size distribution patterns, with perfluorobutanoic acid \(PFBA\) and](#)
100 [PFOA showing variable fine- and coarse-mode enrichment, perfluorobutanesulfonic acid \(PFBS\) generally coarse-dominated,](#)
101 [and PFOS consistently peaking in the 1–10 \$\mu\text{m}\$ range.](#)

102 For example, Dreyer et al. (2015) studied aerosol size distributions in a semi-rural area of Geesthacht, Germany, using a
103 Berner-type cascade impactor (0.14–11.4 μm) and found PFOA mainly associated with ultrafine/submicron particles (< 0.14
104 μm ; within the fine fraction), while PFOS showed enrichment in the supermicron range, particularly 1.4–3.8 μm . Ge et al.
105 (2017) examined indoor and roadside aerosols in Tsukuba, Japan, using a five-stage nano-sampler, and reported ionic
106 perfluoroalkyl carboxylic acids (PFCA) mainly associated with fine particles ($< 0.5 \mu\text{m}$) indoors, while PFOS was enriched in
107 coarse roadside particles (2.5–10 μm). Guo et al. (2018) investigated urban aerosols in Shanghai, China, during a haze period
108 using an eight-stage air sampler, and observed bimodal distributions, with PFOA peaking in both fine (0.4–2.1 μm) and coarse
109 (3.3–10 μm) modes, and PFOS largely associated with coarse particles. Lin et al. (2022) analysed aerosols near wastewater
110 treatment plants and a landfill in Hong Kong, China, using an eleven-stage MOUDI impactor (0.056–10 μm), and found site-
111 dependent patterns: perfluorobutanoic acid (PFBA) and PFOA showed variable fine and coarse mode enrichment,
112 perfluorobutanesulfonic acid (PFBS) was generally coarse-dominated, and PFOS consistently peaked in the 1–10 μm range.

113 These studies provide important data on PFAS size distribution in aerosols; however, the available information remains too
114 limited to establish general patterns or identify the controlling mechanisms. Controlled laboratory investigations, though
115 constrained by simplified conditions and the absence of real-world variability, are therefore needed to disentangle the effects
116 of PFAS molecular structure and interfacial behaviour from the physical processes governing aerosol formation and droplet
117 drying. Such information is critical for improving atmospheric fate models and exposure assessments.

118 The aim of this study was to advance understanding of PFAS aerosol formation and size distribution under controlled
119 laboratory conditions, with particular focus on the potential role of bioaerosols as carriers. In this study, we explore how PFAS
120 with varying carbon chain lengths and functional groups undergo aerosolisation, both in the absence and presence of the model
121 bacterium *Pseudomonas fluorescens*. This bacterium was chosen as it is commonly detected in wastewater and wastewater-
122 impacted matrices, having been isolated from WWTP influent and effluent (including species-level recovery of *Pseudomonas*
123 *fluorescens*), and from raw sewage of municipal treatment plants (phage isolation targeting *Pseudomonas fluorescens*)
124 (Luczkiewicz et al., 2015; Sillankorva et al., 2008). *Pseudomonas fluorescens* is a ubiquitous freshwater bacterium, frequently
125 reported in rivers, lakes, and surface waters, where it occurs in the water column, sediments, and biofilms, supporting its
126 relevance as a representative organism for aquatic and wastewater-influenced systems (Baum et al., 2009; Batrich et al., 2019).

127 Moreover, it presents a low biosafety risk, being classified as a non-pathogenic, Risk Group 1 organism suitable for use in
128 controlled laboratory experiments. Size-resolved PFAS aerosol concentrations were determined for both systems to assess the
129 influence of molecular structure and biological material on particle-phase behaviour. To the best of our knowledge, this is the
130 first study to directly investigate PFAS–bioaerosol interactions and resolve their mass size distribution from polar solvent
131 systems under controlled laboratory conditions.

132 The resulting mass–size distributions were then applied to the Multiple-Path Particle Dosimetry (MPPD) model to evaluate
133 how aerosol size affects potential respiratory deposition and human exposure. Such modelling provides a quantitative context
134 for interpreting the potential health relevance of observed PFAS size distributions.

135 2 Materials and methods

136 2.1 Experimental facility, setup, and conditions

137 The experiments were performed in the Chamber for Aerosol Modelling and Bio-aerosol Research (ChAMBRe) facility at the
138 University of Genoa, Italy. The chamber is a stainless-steel vessel with an internal volume of 2.2 m³, designed for studies of
139 particle generation, ageing, and interaction under controlled environmental conditions (Massabò et al., 2018). All the
140 experiments were conducted at ambient pressure and in dark conditions. Temperature and humidity inside ChAMBRe were
141 continuously monitored and maintained at 23 ± 3 °C and 40 ± 6 %, respectively.

142 Before each experiment, ChAMBRe was evacuated using a composite pumping system (rotary and root pumps) to achieve an
143 internal pressure of approximately 5×10^{-2} mbar. The reestablishment of atmospheric pressure was facilitated by introducing
144 ambient air into the chamber using a five-stage filtration, purification, and drying intake system, which comprised an absolute
145 HEPA filter and a zeolite trap (Vernocchi et al., 2023). A Waveband Integrated Bioaerosol Sensor (WIBS-NEO, Droplet
146 Measurement Technologies®) has been incorporated into the ChAMBRe particle monitoring system to quantify bio-aerosol
147 concentration. The extensive data produced by the WIBS during the ChAMBRe experiments were analysed using custom
148 software developed in Igor 8.0 (Wavemetrics, Inc.), designed to extract airborne bacteria/bioaerosol concentration and size
149 distribution within the chamber as a function of time and fluorescence intensity. In parallel, total particle number and size
150 distributions were monitored in real time using a Scanning Mobility Particle Sizer (SMPS 3938, TSI Inc.) equipped with a
151 differential mobility analyser (DMA 3081A) and a condensation particle counter (CPC 3750) in the range from 18 to 500 nm
152 and an Optical Particle Sizer (OPS, TSI 3330) covering 0.3–10 µm range.

153 2.2 Aerosol generation and introduction

154 2.2.1 PFAS-only experiments

155 A mixed standard solution containing 25 PFAS was prepared using the EPA-533PAR native analyte mixture supplied by
156 Wellington Laboratories (Ontario, Canada). The mixture comprised a broad suite of ionic PFAS, including perfluoroalkyl
157 carboxylic acids (PFCA; C4–C12), perfluoroalkane sulfonates (PFSA; C4, C5, C7 linear, and both linear and branched isomers
158 of C6 and C8), and several fluorotelomer sulfonates and emerging replacement compounds. Specifically, the analyte mixture
159 consisted of: 4:2 fluorotelomer sulfonate (4:2 FTS); 6:2 fluorotelomer sulfonate (6:2 FTS); 8:2 fluorotelomer sulfonate (8:2
160 FTS); hexafluoropropylene oxide dimer acid (HFPO-DA); perfluoro(2-((6-chlorohexyl)oxy)ethanesulfonic acid) (9Cl-
161 PF3ONS); perfluoro(2-ethoxyethane)sulfonic acid (PFEEESA); perfluoro-3-methoxypropanoic acid (PFMPA); perfluoro-3,6-
162 dioxahaepanoic acid (3,6-OPFHpA); perfluoro-4-methoxybutanoic acid (PFMBA); perfluorobutane sulfonic acid (L-PFBS);

Formatted: Superscript

163 perfluorobutanoic acid (PFBA); perfluorodecanoic acid (PFDA); perfluorododecanoic acid (PFDoA); perfluoroheptane
164 sulfonic acid (L-PFHpS); perfluoroheptanoic acid (PFHpA); perfluorohexane sulfonic acid (PFHxS); perfluorohexanoic acid
165 (PFHxA); perfluorooctane sulfonic acid (PFOS); perfluorooctanoic acid (PFOA); perfluorononanoic acid (PFNA);
166 perfluoropentane sulfonic acid (L-PFPeS); perfluoropentanoic acid (PFPeA); perfluoroundecanoic acid (PFUdA); sodium
167 dodecafluoro-3H-4,8-dioxananoate (NaDONA); 11-chloroeicosafluoro-3-oxaundecane-1-sulfonic acid (11Cl-PF3OUdS).
168 All compounds were diluted to a final concentration of 0.5 ng mL⁻¹ in a mixture of 40:60 (v/v) methanol and ultrapure water
169 (18.2 MΩ cm) to ensure adequate solubility and minimise losses to container surfaces.

170 The addition of methanol (≥99.9% (GC), LiChrosolv®, Supelco) was necessary to prevent analyte loss due to sorption onto
171 the nebuliser container walls and to improve the solubility of long-chain PFAS in water. [A 40:60 \(v/v\) methanol-ultrapure](#)
172 [water mixture was used based on prior evidence that methanol additions of approximately 30% \(v/v\) substantially reduce](#)
173 [PFAS losses to glass \(e.g. Mancini et al., 2023\) and polymer surfaces, including glass components of the nebulising system;](#)
174 [the higher methanol fraction was used here to provide a conservative margin accounting for additional losses during](#)
175 [aerosolisation and contact with both glass and stainless steel components of the system. Methanol was selected due to its full](#)
176 [miscibility with water, rapid evaporation during aerosolisation, low background PFAS contamination, and established](#)
177 [compatibility with PFAS analytical workflows \(Kourtchev et al., 2022\), and was used consistently to ensure reproducible](#)
178 [aerosol generation conditions.](#)

179 Aerosols were generated using a three-jet Collison nebuliser operated at 5 L^h min⁻¹ and introduced into ChAMBRé through a
180 stainless-steel inlet connected directly to the chamber. Aerosol generation continued for 30 min, followed by a mixing period
181 of 10 min before sampling, facilitated by the mixing fan installed at the base of the ChAMBRé. The internal fan was operated
182 at 5 Hz, a setting shown by Massabò et al. (2018) to achieve complete mixing in the ChAMBRé within approximately 2 min.
183 Experiments were repeated three times and are referred to as Exp 1-3 (no bacteria) below. Aerosol drying prior to chamber
184 introduction was intentionally avoided to minimise PFAS losses. PFAS are known to interact with surfaces and can partition
185 during drying, so passing the aerosol through additional tubing or drying devices (e.g., diffusion dryers/denuders) would
186 introduce unnecessary interfaces and increase the risk_s of losses. Introducing the wet aerosol directly into the chamber therefore
187 ensured that the measured composition reflected primary aerosol generation rather than processing artefacts. [A simplified](#)
188 [schematic of the experimental setup is shown in Figure S1 of supplement.](#)

189 2.2.2 PFAS and *Pseudomonas fluorescens* experiments

190 The *Pseudomonas fluorescens* ATCC 13525 (obtained from the American Type Culture Collection, University Boulevard,
191 Manassas, Virginia, United States) was grown in 30 mL volume of nutrient broth medium. The culture was incubated at 25°C
192 with continuous shaking in a shaker incubator (SKI 4 ARGOLAB, Carpi, Modena, Italy) at 200 rpm. The growth curve was
193 monitored by measuring the absorbance at $\lambda = 600$ nm using a spectrophotometer (Shimadzu 1900) until it reached the
194 stationary phase (approximately 1) corresponding to about 10⁹ cells mL⁻¹. Subsequently, 20 mL of the bacterial suspension
195 was centrifuged at 5000 rpm for 10 min, and the cell pellet was resuspended in 20 mL of sterile Milli Q (MQ) water.

Formatted: Superscript

Formatted: Superscript

196 The bacteria in MQ were nebulised using Sparging Liquid Aerosol Generator (SLAG) (CH Technologies, USA) with a 0.75”
197 diameter porous disc and nominal pore size of 2 µm. 3 mL of the bacterial suspension with a syringe pump flowrate of 0.4 mL
198 min⁻¹ were dripped onto the SLAG porous stainless-steel disk and nebulised inside ChAMBRe with a flowrate of 3.5 L^h min⁻¹
199 ¹ as performed in previous experiments (Gatta et al., 2025).
200 Bioaerosol was allowed to mix for 5 min, followed by addition of PFAS in the same way as described in 2.2.1. Aerosol
201 generation continued for 30 min, followed by a mixing period of 10 min before sampling. Experiments were repeated three
202 times and are referred to as Exp 4-6 (with bacteria) below.

203 2.2.3 Blank experiments

204 Blank experiments were conducted to assess potential contamination or background levels arising from the experimental setup
205 and to correct for any systematic bias in the measurements. A 40:60 (v/v) methanol–ultrapure water mixture without PFAS
206 was nebulised using a Collision nebuliser at 5 L min⁻¹. Aerosol generation was maintained for 30 min, followed by a 10 min
207 mixing period prior to sampling. All other experimental conditions were identical to those described in Section 2.2.1. The
208 blank experiments were repeated three times.

209 2.3 Aerosol generation and introduction

210 Size-segregated aerosol samples were collected using a Nano Micro-Orifice Uniform Deposit Impactor (NanoMOUDI-IITM,
211 Model 125B, MSP Corporation, USA) operated at a flow rate of 10 L min⁻¹. The NanoMOUDI provided aerodynamic cut-off
212 diameters of 10.000, 5.600, 3.200, 1.800, 1.000, 0.560, 0.320, 0.180, 0.100, 0.056, 0.032, 0.018, and 0.010 µm.

213 Total suspended particles (TSP) were collected in parallel with a double cone sampler, directly connected to ChAMBRe, at a
214 flow rate 10 L min⁻¹. The total sampling duration for both NanoMOUDI and TSP was 2 hours.

215 PallFlex 2500 QAO-UP quartz fibre filters were used as substrates in both samplers. Due to the unavailability of PallFlex 2500
216 QAO-UP filters for all experiments, quartz microfibre filters (RVMSFQ47Q90, Mega Systems s.r.l.) were used in TSP
217 sampling in one of the replicate experiments involving bacteria. All filters were prebaked at 450 °C for 2.5 hours prior to
218 sampling. Based on recoveries and variability between TSP replicates (RSD < 10%), which was not higher than that observed
219 for replicates using the same filter type, the use of a different filter brand is expected to have a negligible impact on the results.
220 Following sampling, aerosol samples were wrapped into aluminium foil (prebaked at 450 °C for 2 hours) avoiding contact
221 with any plasticware and external environment and stored approximately for 60 days at –20 °C until extraction.

222 2.4 PFAS extraction and analysis

223 Samples generated in the chamber were extracted and analysed following the procedure described by Kourtchev et al. (2022).
224 Briefly, filter edges in contact with the sampler gaskets were removed prior to extraction. Each filter was placed in a precleaned
225 10 mL glass vial (Chromacol 10-HSV, Thermo Scientific) and spiked with 25 µL of an internal standard (IS) mixture
226 containing 16 isotopically labelled (¹³C) PFAS at 1 ng mL⁻¹ and three telomer sulfonates (M2-4:2 FTS, M2-6:2 FTS, and M2-

Formatted: Superscript

227 8:2 FTS) at 4 ng mL⁻¹. Full names of the isotopically labelled PFAS are shown in Table S1 of supplement. Samples were
228 extracted twice with 5 mL of Liquid Chromatography Mass Spectrometry (LC-MS, CHROMASOLV™ $\geq 99.9\%$) grade
229 methanol using ultrasonic agitation in a chilled water bath for a total of 40 min (2 × 20 min). The combined extracts were
230 filtered through PTFE membrane filters (0.45 μm, Iso-Disc PTFE-13-4) into prewashed 10 mL glass vials (Chromacol 10-
231 HSV) tightly closed with metal screw caps and PTFE septa (Chromacol 18-MS and 18-ST101).

232 Extracts were then reduced in volume to 1 mL under a gentle stream of nitrogen and stored at 4 °C until analysis. On the day
233 of analysis, 4 mL of Optima™ LC-MS grade water was added to each sample, which was subsequently vortex-mixed and
234 analysed using online SPE consisting of an EQuan MAX Plus Thermo Scientific™ Vanquish™ UHPLC system equipped with
235 a Thermo Scientific™ TriPlus™ RSH autosampler, following the method described by Kourtchev et al. (2022). All samples
236 were analysed within 24 hours of extraction for each analytical batch.

237
238 Only PFAS detected above the method's LOD (Kourtchev et al., 2022) or above blank levels were considered in the data
239 interpretation. All data were corrected for chamber dilution to account for the continuous inflow of clean air required to
240 maintain stable chamber pressure. Direct quantification of aerosol-phase PFAS wall losses was not performed, as it would
241 require time-resolved aerosol-phase PFAS measurements that are not technically feasible at the concentrations applied, given
242 the absence of online measurement techniques for ionic PFAS and the need for extended offline sampling to achieve sufficient
243 analytical sensitivity, especially in size-resolved samples. No correction was applied for potential chamber wall losses. Because
244 the chamber and associated lines are made of stainless steel, and long-chain PFAS are known to interact strongly with metal
245 surfaces, additional losses to the walls are likely and may contribute to the overall uncertainty. However, as all experiments
246 were conducted under the same conditions, any wall-loss effects are expected to be systematic and should not affect the relative
247 comparison of the results. Moreover, wall-loss efficiencies may vary with PFAS chain length and could influence absolute
248 recoveries. All experiments were therefore conducted under consistent chamber configuration and operating conditions to
249 minimise variability in wall-loss behaviour and to allow relative comparisons within a common experimental framework.

250 2.5 Multiple-Path Particle Dosimetry (MPPD) modelling

251 For each region of the human respiratory tract (Head, Tracheobronchial region (TB) and Pulmonary region(P), the deposition
252 efficiency as a function of particle size, was estimated using the MPPD model (version 2.11, Applied Research Associates,
253 Inc.) (Anjilvel and Asgharian, 1995), using the default human breathing parameters (further details and results are provided
254 in the supplement file). The MPPD model is based on a framework of semiempirical equations and computational algorithms
255 that simulates particle deposition in the respiratory tract using anatomical and physiological data. It accounts for species-
256 specific airway geometry, breathing patterns, and particle characteristics to estimate regional and total deposition under various
257 exposure scenarios.

258 The deposition flux, $DF_{r,i}$ (pg h⁻¹) to each region of the human respiratory tract (Head, TB or Pulmonary), r , for each
259 nanoMOUDI size bin, i (assuming constant exposure), was then calculated as

260

$$DF_{r,i} = DE_{r,i} \times C_i \times V$$

261 where $DE_{r,i}$ is the deposition efficiency, C_i ($\mu\text{g m}^{-3}$) is the measured concentration of the target PFAS and V ($\text{m}^3 \text{h}^{-1}$) is the
262 human breathing rate. The deposition fluxes for the coarse ($> 2.5 \mu\text{m}$), fine ($0.1 - 2.5 \mu\text{m}$), and ultrafine ($< 0.1 \mu\text{m}$) size
263 fractions were then calculated by summing across the relevant MOUDI size bins.

264 3 Results and Discussions

265 3.1 Total suspended particles (TSP)

266 Figure 1 shows concentration of individual PFAS measured in the TSP fraction for the PFAS-only (Exp 1–3) and PFAS with
267 *Pseudomonas fluorescens*-seeded (Exp 4–6) experiments.

268 Distinct trends were observed between the sulfonated and carboxylated PFAS. The sulfonated compounds, i.e. PFBS, PFHxS,
269 PFOS, and the fluorotelomer sulfonates (4:2, 6:2, and 8:2 FTS), exhibited relatively uniform aerosol-phase concentrations,
270 indicating that chain length had little influence on their aerosolisation efficiency. Their consistent behaviour likely reflects the
271 inherently high surface activity of sulfonates, which promotes their enrichment at the air water interface (Klevan et al., 2025;
272 Lyu et al., 2022).

273 In contrast, the PFCA showed a clear chain-length dependence, with aerosol-phase concentrations increasing from PFBA to
274 PFUDA. In a 40:60 methanol-water system, methanol decreases surface tension and solvent polarity, enhancing the solubility
275 and mobility of longer-chain PFCA relative to pure water (Kutsuna et al., 2012). This mixed-solvent environment therefore
276 favours the transfer of hydrophobic carboxylates into the aerosol phase. It must be noted that short-chain PFAS e.g. PFBA
277 (C_3) are less surface active and can remain in solution (Cai et al., 2022; Klevan et al., 2025). While a clear chain-length-
278 dependent increase in aerosol-phase PFCA concentrations is observed, any preferential wall losses of longer-chain compounds
279 would act to reduce their measured recovery and therefore bias the magnitude of this increase towards lower values.

280 Accordingly, sulfonated PFAS appear dominated by interfacial adsorption, whereas carboxylated PFAS are more strongly
281 affected by bulk-phase solvation governed by solvent composition. While direct comparison with earlier studies is limited by
282 methodological differences, similar behaviour has been observed during water aeration, where perfluoro sulfonated
283 compounds exhibited higher aerosolisation efficiencies than carboxylated analogues (Pandamkulangara Kizhakkethil et al.,
284 2024; Pandamkulangara Kizhakkethil and Kourtchev, 2025). A similar trend, involving an increase in aerosol-phase
285 perfluorinated alkyl acids, their salts and conjugate bases abundance with perfluoroalkyl chain length but not equivalent
286 enrichment magnitudes, was also observed under highly aqueous (tap water) conditions in bubble-bursting experiments using
287 a plunging jet, which is considered representative of nascent sea spray aerosol formation, as reported by Reth et al. (2011).

288 In the presence of *Pseudomonas fluorescens* (Fig. 1, Exp 4–6), the overall TSP concentrations of most PFAS were comparable
289 to those in the PFAS-only experiments, indicating that bacterial seeds did not substantially influence PFAS aerosolisation
290 under the tested conditions. The average and standard deviation of bacteria concentration across the 3 replicated experiments,
291 measured by WBS, 5 minutes after the end of injection was $29 \pm 1 \# \text{cm}^{-3}$. Slight reductions observed for some long-chain

292 PFCA (e.g. PFNA, PFDA, PFUdA) may reflect weak sorptive interactions with bacterial cell walls or their fragments, although
293 these effects appear minor relative to the dominant physicochemical controls. The overlap of standard deviations between the
294 two experimental conditions (with and without *Pseudomonas fluorescens*) suggests that PFAS concentrations in aerosol were
295 similar within the experimental uncertainty.

296 It must be noted that the major fraction of *Pseudomonas fluorescens* present in the chamber was observed around 0.6 μm
297 (Figure 2), smaller than the typical bacterial dimension (about 2-4 μm in length and 0.5-1.0 μm in diameter). It is worth noting
298 that the nebulisation processes exert stress on bacteria, producing fragmentation (Park et al., 2009). Particles in this size range
299 lie within the accumulation mode and therefore may act as efficient condensation sinks for condensable species (Engvall et
300 al., 2008). In the present experiments, PFAS were introduced in ionic form via nebulisation, yielding PFAS in both the gas
301 phase and the particle phase (the latter associated with nebulised droplets and their dried residues). Any enrichment of PFAS
302 on the pre-existing bacterial particles would therefore have required gas-particle partitioning to the bacterial surface or
303 particle-particle interactions such as coagulation. The absence of measurable enhancement in PFAS aerosol concentrations
304 therefore suggests that condensation or adsorption of PFAS onto bacterial surfaces was not thermodynamically favourable, or
305 that kinetic limitations prevented significant mass transfer during the experimental timescale. This suggests that, under the
306 applied conditions, PFAS aerosol formation and growth were predominantly governed by nebulisation and subsequent droplet
307 drying processes rather than by heterogeneous uptake onto biological particles.

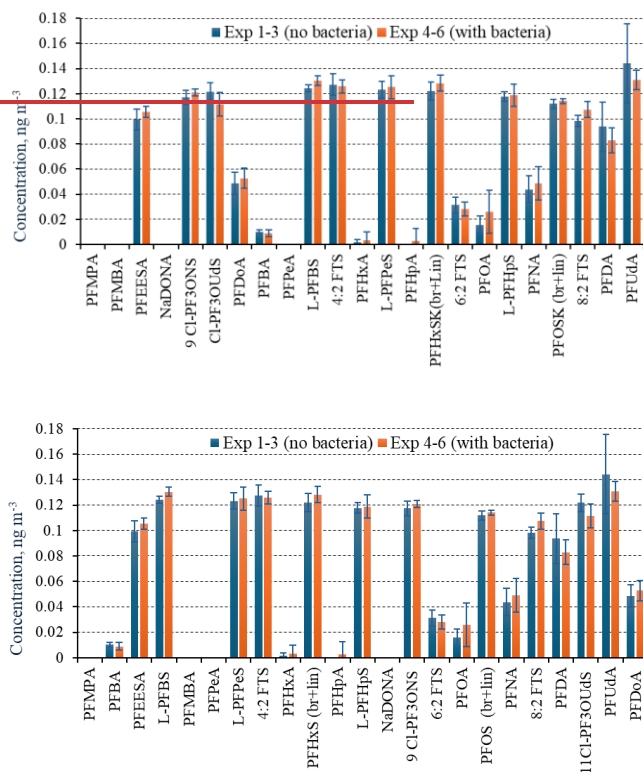
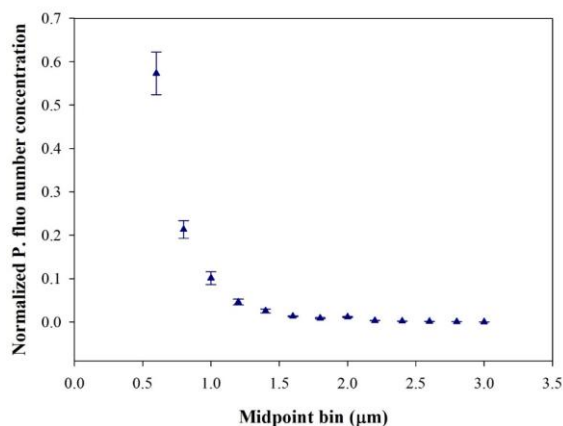


Figure 1: Aerosol-phase concentrations of individual PFAS measured in total suspended particles (TSP) during PFAS-only experiments (Exp 1-3, blue) and PFAS + *Pseudomonas fluorescens*-seeded experiments (Exp 4-6, orange). Error bars show the standard deviation across three chamber replicates with duplicate LC-MS analyses per replicate (n = 6). PFAS are arranged along the x axis according to carbon chain length. Overall, similar aerosol-phase PFAS concentrations are observed with and without biological material, indicating no systematic bacterial influence.



315

316 Figure 2: Normalised particle size distribution of *Pseudomonas fluorescens* nebulised in ChAMBRe (5 minutes after the end of
 317 bacteria nebulisation). Data represent the mean \pm standard deviation of three replicate experiments. The dominant fraction of
 318 *Pseudomonas fluorescens* present in the chamber was observed around 0.6 μm .

319 3.2 Mass–Size Distributions of PFAS

320 As mentioned in the Methodology section, not all PFAS detected in the TSP samples were also observed in the NanoMOUDI
 321 samples, with carboxylated PFAS being mainly affected. This was likely due to their lower aerosol concentrations in the
 322 chamber (as also observed in TSP) and their generally higher volatility (e.g. PFBA, 6.37 mmHg at 25 °C, Steele et al., 2002;
 323 PFHxA, 13 mmHg at 25 °C, US EPA, 2012), which reduce particle-phase partitioning. Additionally, “dilution” across multiple
 324 MOUDI stages may have further contributed to concentrations falling below the LC-MS detection limit in the NanoMOUDI
 325 samples.

326 The majority of PFAS (excluding 6:2 FTS and PFOS) aerosols exhibited a consistent unimodal mass–size distribution, peaking
 327 at 0.32 μm (Figure 3). Interestingly, variations in the molecular composition of the tested PFAS, including differences in
 328 perfluorocarbon chain length and terminal functional group, did not affect the mode diameter of the aerosol mass–size
 329 distribution. PFAS, representing a broad range of compounds, differ markedly in hydrophobicity and interfacial activity as a
 330 function of both chain length and functional group (e.g. Lyu et al., 2022; Patel et al., 2024; Leung et al., 2023), which makes
 331 the present observation somewhat unexpected. For instance, long-chain sulfonates such as PFOS (C8) exhibit considerably
 332 stronger surface activity than short-chain carboxylates such as PFBA (C3), and their behaviour in bulk aqueous systems differs
 333 accordingly (Guo et al., 2023).

334 This suggests that, under the applied experimental conditions, aerosol formation and size characteristics were largely governed
 335 by physical processes. The most plausible explanation is that the aerosol-generation method imposed uniform physical

336 constraints during droplet formation and solvent evaporation, limiting the extent to which molecular properties influenced
337 particle characteristics. In addition, the use of an organic solvent likely enhanced the solubility of all PFAS, including long-
338 chain species with low water solubility, allowing them to remain in solution and aerosolise more uniformly during nebulisation.
339 Methanol substantially reduces surface tension (from 71.7 dyne cm⁻¹ for pure water to 38.7 dyne cm⁻¹ at 40 % v/v methanol
340 at 25 °C; Cheong and Carr, 1987), which promotes droplet formation and minimises differences in surface activity among
341 PFAS, thereby obscuring potential molecular-specific effects on aerosol behaviour.

342 The two analytes, 6:2 FTS and PFOS, did not follow the general mass-size distribution trend. Although PFOS exhibited a
343 dominant submicron mass mode at 0.32 µm, similar to other PFAS, its mass-size profile showed a relatively larger fraction of
344 mass in the smallest measured bins. In other words, PFOS retained the common 0.32-µm residual peak but also displayed
345 enrichment in the ultrafine fraction compared with other PFAS in the mixture. PFOS may produce a larger fraction of ultrafine
346 aerosol particles than other PFAS due to its greater surface activity (Klevan et al., 2025; Lyu et al., 2022). Although the
347 presence of methanol substantially reduces bulk surface tension, PFOS can still dominate dynamic interfacial processes during
348 rapid droplet formation. Its strong and persistent adsorption at the air-liquid interface, combined with enrichment as methanol
349 evaporates, likely lowers local surface tension further and inhibits coalescence, resulting in smaller and more stable droplets.
350 In addition, the anionic nature of PFOS may contribute to electrostatic stabilisation of charged droplets, further enhancing the
351 ultrafine fraction.

352 Other long-chain PFAS in the mixture did not exhibit similar enrichment, potentially due to competitive adsorption and
353 intermolecular interactions in mixtures that modulate their effective surface activity.

354 Only a limited number of studies have reported size-resolved mass distributions of PFAS associated with atmospheric particles
355 from the field observations. Comparison with previous work shows that PFAS size distributions vary considerably among
356 studies. Harada et al. (2006) and Dreyer et al. (2015) reported compound-dependent patterns, with PFOA and other PFCA
357 enriched in fine or ultrafine particles, whereas PFOS tended to occur in coarser fractions. In contrast, Guo et al. (2018) found
358 both PFOA and PFOS primarily associated with fine particles (< 1 µm), while Ge et al. (2017) observed PFCA in ultrafine
359 particles (< 0.1 µm) and PFOS and other sulfonates in coarse modes. Such variability likely reflects differences in sources,
360 atmospheric conditions, and sampling methodologies, as well as local physicochemical environments influencing PFAS
361 partitioning.

362 To the best of our knowledge, previous laboratory investigations of PFAS aerosol size behaviour have focused primarily on
363 sea-spray systems, which are not directly comparable to the organic solvent-rich aerosolisation process examined here.
364 Johansson et al. (2019) reported that the highest enrichment of perfluoroalkyl acids (PFCA) relative to seawater occurred in
365 aerosols with aerodynamic diameters below 1.6 µm. Sha et al. (2021) found that particle surface-area-to-volume ratio was a
366 strong predictor of PFAS enrichment in supermicron particles but not in submicron particles, indicating that different physical
367 controls operate across size ranges. In their subsequent work, Sha et al. (2024) observed that PFAS enrichment was particularly
368 pronounced in submicrometer sea-spray aerosol particles and varied with chain length and dissolved organic matter content.
369 These studies suggest that in marine systems, PFAS enrichment and size association are sensitive to experimental conditions

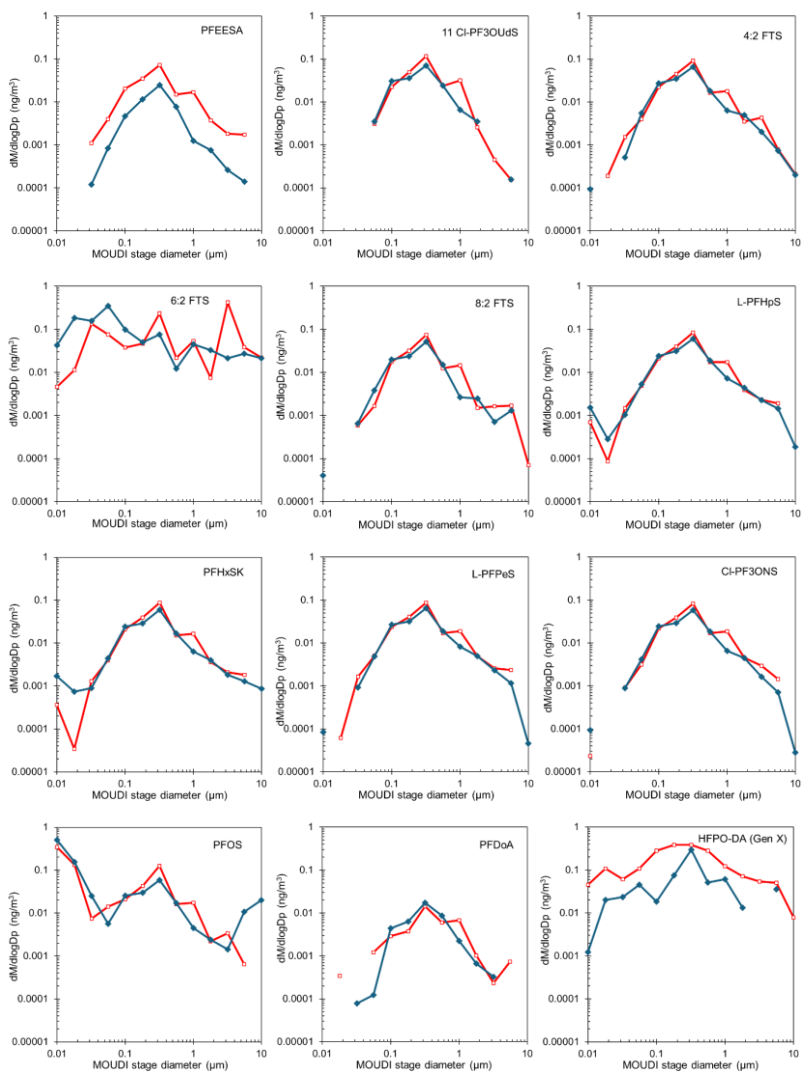
370 and molecular structure, with both particle-scale physics and surfactant properties influencing partitioning. In contrast, the
371 consistent submicron unimodal distribution observed in the present work likely reflects aerosol formation under organic-
372 solvent conditions, where rapid solvent evaporation and solute concentration effects impose dominant physical constraints that
373 reduce the influence of PFAS molecular features on particle size.

374 The introduction of *Pseudomonas fluorescens* into the chamber as a potential seed or carrier of PFAS, in most cases, had either
375 no effect (within experimental error) or resulted in a uniform decrease in PFAS aerosol mass size concentration across nearly
376 the entire size range for two analytes (i.e. PFEESA and GenX), while the distribution profile and modal diameter remained
377 unchanged. As mentioned in the section 3.1, the major fraction of *Pseudomonas fluorescens* in the chamber was observed
378 around 0.6 μm (Fig 2). The absence of PFAS enrichment at the bacterial modal size ($\sim 0.6 \mu\text{m}$) and the unchanged PFAS modal
379 diameter ($\sim 0.3 \mu\text{m}$) indicate that *Pseudomonas fluorescens* did not noticeably influence PFAS size distribution under the tested
380 conditions. This was somewhat unexpected, as PFAS have been shown to associate with bacterial surfaces in aqueous systems
381 (Dai et al., 2023). The physicochemical environment in aerosols likely may differ from that in bulk water. The outer membrane
382 of *Pseudomonas fluorescens* carries a net negative charge, arising from acidic functional groups on lipopolysaccharides and
383 phospholipids (Boyd Chelsea et al., 2014; Charlton et al., 2024), while the tested PFAS are also anionic. Such electrostatic
384 repulsion could therefore further inhibit PFAS attachment, potentially explaining the absence of observable enrichment at ~ 0.6
385 μm . In addition, although PFAS are amphiphilic, their molecular structure makes the air–water interface far more favourable
386 for stabilisation than the hydrated, negatively charged bacterial surface, and PFAS therefore likely preferentially stabilise at
387 droplet interfaces rather than adsorb onto bacterial cells. Another aspect worth considering is whether *Pseudomonas*
388 *fluorescens* could have influenced PFAS aerosol concentrations through biochemical transformation rather than solely through
389 physical carrier processes. In bulk aqueous systems, several *Pseudomonas* species have been reported to partially degrade
390 sulfonated PFAS, particularly precursors such as H-PFOS, under nutrient-enriched or co-metabolic conditions (e.g., Key et
391 al., 1998). The latter work involved liquid culture media with high bacterial densities, organic carbon co-substrates, and
392 prolonged incubation times, which facilitate enzymatic activity and redox transformations. However, even in that study,
393 evidence for complete degradation of PFOS is lacking; rather, transformation is slow, partial, and often requires co-metabolic
394 drivers. By contrast, the conditions in our aerosol chamber differ fundamentally. The bacteria were suspended in air with
395 transient water content (RH \sim 40%), rather than immersed in nutrient-rich aqueous media. Under such conditions, the metabolic
396 activity of *Pseudomonas fluorescens* is expected to be extremely limited. The observed uniform decrease in PFAS aerosol
397 mass concentration cannot therefore be straightforwardly attributed to microbial degradation, as the air–water interface-
398 dominated microenvironment is unlikely to sustain enzymatic pathways known to act on PFAS in bulk liquid cultures.
399 Furthermore, the residence time of particles in the chamber is orders of magnitude shorter than the timescales over which
400 reported PFAS transformations by *Pseudomonas* occur (days to weeks). It is therefore more plausible that the apparent decrease
401 in GenX and PFEESA aerosol mass concentrations reflect non-biological processes such as redistribution of material to
402 chamber or sampler walls, or surface-competition dynamics during condensation, rather than direct microbial influence. If any
403 biochemical contribution occurred, it would likely be negligible compared with these physicochemical pathways. The

404 difference in TSP concentrations between the *Pseudomonas fluorescens*-seeded (average $0.105 \pm 0.0043 \text{ ng m}^{-3}$, $n=3$) and
405 unseeded ($0.099 \pm 0.008 \text{ ng m}^{-3}$, $n=3$) experiments for PFEESA was minimal, suggesting that the concentration drop observed
406 in the NanoMOUDI size-resolved data likely resulted from sampling artefacts or volatility-driven size redistribution rather
407 than bacterial activity. In this respect, it has been shown that compounds with higher volatility tend to exhibit greater mass
408 losses through evaporation particularly in impactor-based sampling systems like NanoMOUDI (e.g. Ungeheuer et al., 2022).
409 Although the same inferences could not be made for GenX from the TSP data, due to high background levels in the TSP
410 blanks, evaporation from the collection substrate in the NanoMOUDI was likely the dominant loss process, as also suggested
411 for PFEESA. The relatively high vapour pressure of GenX (2.7 mm Hg at 20 °C, US EPA, 2022) supports this interpretation.
412 In previous work, it was found that the culturable lifetime of *Pseudomonas P. fluorescens* in ChAMBRé in dark condition was
413 about 20 minutes (Gatta et al. 2025). Furthermore, the survival of bacteria in air is known to be sensitive to aerosolisation and
414 sampling conditions rather than simply liquid-phase growth (Després et al., 2012; Hong et al., 2021). It must be noted that in
415 our study the bacteria were seeded in sterilised MQ, whereas PFAS were introduced separately via a 40:60 (v/v) methanol-
416 water nebulisation. Under this experimental setup, bacteria were not subjected to high alcohol strength in the droplet phase;
417 instead, their methanol exposure was dominated by chamber-average vapour and sporadic interactions near the spray plume.
418 These conditions are unlikely to produce strong biocidal effects at the population level, so the absence of PFAS enrichment at
419 the bacterial size mode is better explained by interfacial/partitioning constraints than by methanol-induced loss of viability.
420 Moreover, even if a fraction of the bacterial population experienced viability loss, this would not preclude potential PFAS
421 interactions with biological surfaces. Non-viable bacterial cells, cell-wall fragments, and microbial biomass retain abundant
422 functional groups (carboxyl, phosphate, and amine moieties) known to sorb organic and inorganic species (Fathollahi [and](#)
423 [Coupe, 2021](#); [Torres, 2020](#); [Wang and](#) [Chen, 2009](#)). Inactivated bacterial biomass is widely used as a biosorbent due to
424 preserved surface chemistry and polymeric matrices ([Torres 2020](#)). In the atmosphere, biological particles occur not only as
425 intact cells but also as cell fragments and exudates ([Després et al., 2012](#); [Fröhlich-Nowoisky et al., 2016](#)), meaning that surface
426 area and chemical functionality persist even when viability is compromised. Thus, even partial loss of viability would still
427 permit association of PFAS with microbial surfaces if interfacial partitioning were favourable. The lack of detectable PFAS at
428 the bacterial size mode therefore reinforces that limited affinity/partitioning, rather than loss of cellular integrity, governed
429 PFAS–bioaerosol interactions under our experimental conditions. [We emphasise that in environmental systems where PFAS](#)
430 [and biological matter may also be internally mixed in aqueous sources prior to droplet formation, different interaction](#)
431 [mechanisms may occur.](#)

Formatted: Superscript

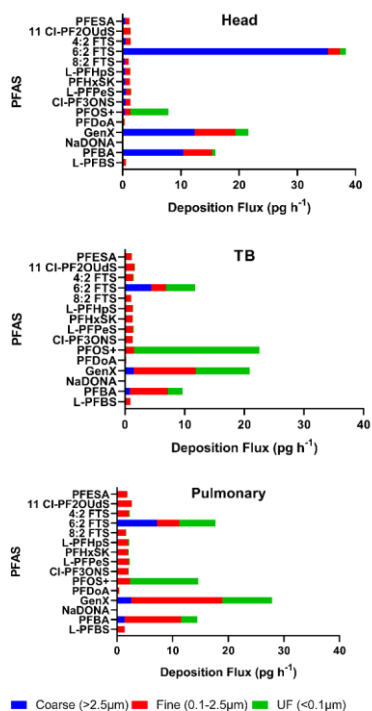
Formatted: Superscript



434 Figure 3: Mass size distribution of aerosol from PFAS-only (blue symbols) and PFAS with *Pseudomonas fluorescens* seed (red
 435 symbols) experiments. Most PFAS exhibit a unimodal mass-size distribution centred near 0.3 μm , indicating dominant fine-mode
 436 aerosol association across compounds.

437 3.3 Multiple-Path Particle Dosimetry (MPPD) modelling

438 Figure 4 (with data given in the supplement) presents the deposition fluxes across respiratory regions (head, TB, pulmonary)
 439 and the relative contributions of inhaled PFAS associated with coarse, fine, and ultrafine particles. The majority of PFAS
 440 measured exhibited similar size distributions, with most particles falling within the fine fraction (0.1 – 2.5 μm), resulting in
 441 broadly consistent deposition patterns. The average total deposition flux across these PFAS was $5.3 \pm 1.0 \text{ pg h}^{-1}$, with
 442 deposition distributed relatively evenly between the head ($23\% \pm 2\%$, 1.22 pg h^{-1}), TB ($26\% \pm 1\%$, 1.34 pg h^{-1}), and pulmonary
 443 ($40\% \pm 1\%$, 2.08 pg h^{-1}) regions.



444
 445 Figure 4: Modelled fractional deposition flux (pg h^{-1}) in the Pulmonary, Tracheobronchial (TB) and Head regions of the human
 446 respiratory tract.

447 PFDoA and NaDONA were notable exceptions due to their significantly lower aerosol concentrations, resulting in total
448 deposition fluxes of 1.18 pg h^{-1} and 0.138 pg h^{-1} , respectively. PFDoA's size distribution was similar to the majority, yielding
449 comparable regional deposition: 29% to the head (0.34 pg h^{-1}), 22% to the TB region (0.26 pg h^{-1}), and 36% to the pulmonary
450 region (0.43 pg h^{-1}). NaDONA however exhibited an additional peak in the coarse fraction, shifting deposition toward the head
451 region, which received 57% of the total flux (0.08 pg h^{-1}), while the TB and pulmonary regions received 13% (0.02 pg h^{-1}) and
452 21% (0.03 pg h^{-1}), respectively. PFOS and PFBA showed significantly higher aerosol concentrations, with total deposition
453 fluxes of 48.1 pg h^{-1} and 44.3 pg h^{-1} , respectively. PFBA had a similar size distribution to the majority but at higher
454 concentration, resulting in deposition fractions of 36% to the head (15.9 pg h^{-1}), 22% to the TB region (9.7 pg h^{-1}), and 33%
455 to the pulmonary region (14.5 pg h^{-1}). PFOS, however, had an additional peak in the ultrafine range, shifting deposition toward
456 the TB region, which received 47% of the total flux (22.5 pg h^{-1}), while the head region received 16% (7.9 pg h^{-1}). GenX and
457 6:2 FTS exhibited the highest aerosol concentrations and deposition fluxes, at 77.5 pg/h and 74.4 pg h^{-1} , respectively. GenX
458 followed the typical deposition pattern, with 28% to the head (21.6 pg h^{-1}), 27% to the TB region (20.9 pg h^{-1}), and 36% to the
459 pulmonary region (27.9 pg h^{-1}). In contrast, 6:2 FTS had additional modes in both the ultrafine and coarse fractions, leading to
460 a deposition profile skewed toward the head region, which received 52% of the total flux (38.4 pg/h), while the TB and
461 pulmonary regions received 16% (11.8 pg h^{-1}) and 24% (17.7 pg h^{-1}), respectively. This pattern was similar to that observed
462 for NaDONA.

463 Particle deposition in the respiratory tract is primarily governed by inertial impaction, gravitational sedimentation, and
464 Brownian diffusion, each dominating in different regions depending on particle size and airflow. Coarse particles deposit
465 mainly in the upper airways via impaction and sedimentation, while ultrafine particles reach the distal pulmonary region
466 through diffusion. Modelled deposition efficiencies by size and region are provided in the SI. Comparing the relative
467 contribution to the deposition flux of the inhaled PFAS associated with the different size fractions, coarse particles showed the
468 highest deposition flux in the head region ($60\% \pm 3\%$), with lower contributions to the pulmonary ($15\% \pm 2\%$) and
469 tracheobronchial ($3\% \pm 8\%$) regions. Fine particles ($0.1\text{--}2.5 \mu\text{m}$), which dominate the PFAS size distribution, had the lowest
470 overall deposition efficiency but were more evenly distributed: $39\% \pm 10\%$ to the pulmonary region, $25\% \pm 7\%$ to TB, and
471 $18\% \pm 5\%$ to the head. Ultrafine particles shifted deposition toward the pulmonary region ($45\% \pm 14\%$), with $35\% \pm 11\%$ to
472 TB and only $8\% \pm 3\%$ to the head.

473 The modelled deposition behaviour of PFAS compounds investigated is closely linked to their particle size distribution. PFOS,
474 GenX, 6:2 FTS, and PFBA exhibited significant ultrafine fractions, suggesting a higher likelihood of deep lung penetration.
475 This is particularly concerning given that clearance mechanisms in the pulmonary region are slower compared to upper
476 airways, and pulmonary deposition increases the potential for translocation into the bloodstream. These findings highlight the
477 importance of considering both particle size and regional deposition when assessing inhalation exposure risks, especially for
478 compounds with known toxicological profiles and environmental persistence. The modelling is not intended to represent
479 population-level exposure or the full range of environmental conditions, but rather to evaluate size-resolved respiratory
480 deposition behaviour for the measured aerosol populations.

481 4 Conclusions

482 This study examined the aerosol formation and size-resolved distribution of a range of PFAS under controlled chamber
483 conditions, using mixed water–organic systems with and without the model bacterium *Pseudomonas fluorescens* to assess the
484 influence of molecular structure, interfacial behaviour and biological material on aerosol properties.

485 In terms of aerosolisation efficiency, sulfonated PFAS exhibited broadly similar aerosol-phase concentrations across chain
486 lengths, whereas perfluoroalkyl carboxylic acids showed increasing aerosolisation with increasing chain length, highlighting
487 the influence of functional group and hydrophobicity on the overall transfer of PFAS into the particle phase.

488 Most PFAS were associated with the fine aerosol mode, displaying unimodal mass–size distributions centred near 0.3 μm .
489 This consistent fine-mode behaviour across PFAS of differing chain lengths and functional groups indicates that aerosol
490 formation was governed primarily by physical processes of droplet generation and evaporation. PFOS showed enhanced
491 ultrafine enrichment, while 6:2 FTS and NaDONA displayed broader profiles, suggesting that differences in volatility and
492 interfacial behaviour introduce secondary compound-specific effects.

493 The presence of *Pseudomonas fluorescens* as an aerosol seed did not enhance PFAS aerosolisation or alter modal diameters,
494 but resulted in small, compound-specific reductions, particularly for PFEESA and GenX. The absence of PFAS enrichment at
495 the bacterial modal diameter ($\sim 0.6 \mu\text{m}$) indicates limited association of PFAS with bacterial surfaces under the tested
496 conditions, likely reflecting electrostatic repulsion and preferential stabilisation of PFAS at air–liquid interfaces. These results
497 suggest that biological material exerts only a minor influence on PFAS partitioning through the airborne pathway examined
498 here; however, aqueous-phase sorption or complexation before aerosolisation may still contribute to water-to-air transfer and
499 warrants further investigation. Moreover, if similar behaviour holds in the atmosphere, surface-active PFAS may avoid shifting
500 into bioaerosol particle sizes with higher deposition velocities and therefore remain in the fine aerosol range with longer
501 atmospheric lifetimes and transport potential.

502 MPPD simulations using the experimental size distributions indicated that most aerosol-bound PFAS would deposit in the
503 pulmonary region. Compounds with stronger ultrafine enrichment, including PFOS, 6:2 FTS and GenX, showed higher
504 predicted deposition in distal lung regions where clearance is slow and transfer into epithelial lining fluids is more likely.

505 Under the studied conditions, PFAS-containing aerosols therefore fall largely within respirable size ranges relevant to
506 inhalation exposure. It must be noted that MPPD modelling serves to contextualise size-resolved respiratory deposition for the
507 observed aerosol populations, not to represent population-level exposure or comprehensive environmental scenarios. However,
508 our results can be used as reference points for future field measurements and for evaluating the relevance of different aerosol
509 generation processes that produce similar particle size ranges.

510 Overall, PFAS aerosolisation and particle-phase behaviour in the mixed solvent system were dominated by the physical
511 processes of droplet formation and evaporation, suggesting that engineering and operational measures that suppress fine droplet
512 production could reduce airborne PFAS emissions. The observed fine-mode distributions also imply that aerosolised PFAS
513 may be efficiently transported in the atmosphere and contribute to inhalation exposure beyond immediate emission sources.

514 Although the water–methanol system does not fully reflect environmental conditions, it provides a controlled basis for
515 identifying the fundamental processes governing PFAS transfer from contaminated aqueous systems to air. [Variability in](#)
516 [temperature and relative humidity may influence PFAS aerosol behaviour through effects on aerosol water content and](#)
517 [evaporation dynamics and should be considered when extrapolating these findings to broader atmospheric conditions.](#)
518 Future work should apply this framework to more environmentally representative matrices, including natural organic matter,
519 and diverse microbial assemblages, to better capture real emission complexity. Combining controlled chamber experiments
520 with field measurements of size-resolved PFAS and bioaerosol emissions will be essential for improving predictions of PFAS
521 atmospheric transport, deposition and human exposure.

522 **5 Financial Support**

523 This work was supported by the European Commission, Horizon 2020 Research Infrastructures (EUROCHAMP-2020) Trans
524 National Access grant ATMO-TNA-6M-0000000034, “Investigation of the aerosolisation dynamics and biological
525 interactions of GenX “forever chemicals” – AEROBIOGEN”. The authors gratefully acknowledge the Coventry University
526 QR funding for supporting the Trailblazers PhD studentship awarded to JPK, secured by IK, and also thank CAWR at Coventry
527 University for its financial assistance.

528 **6 Competing Interests**

529 Some authors are members of the editorial board of journal ACP. The authors have no other competing interests to declare.

530 **7 Author Contributions**

531 IK, SC, FM, EG, DM, PP conceived the study. IK, JPK, SC, FM, DM, EG, VV performed lab measurements, sampling, and
532 sample analysis. IK, JPK, FM, EG performed data processing and interpretation. AB performed modelling. IK, JPK, FM, AB
533 prepared the original draft of the paper. All authors contributed to reviewing and editing the manuscript.

534 **8 Data Availability**

535 The dataset for this work can be accessed at DOI 10.5281/zenodo.17756209

536 **9 References**

- 537 Ahrens, L., Shoeb, M., Harner, T., Lee, S. C., Guo, R., and Reiner, E. J.: Wastewater Treatment Plant and Landfills as Sources
538 of Polyfluoroalkyl Compounds to the Atmosphere, *Environ. Sci. Technol.*, 45, 8098-8105, <https://doi.org/10.1021/es1036173>,
539 2011.
- 540 Alves, A. V., Tsianou, M., and Alexandridis, P.: Fluorinated Surfactant Adsorption on Mineral Surfaces: Implications for
541 PFAS Fate and Transport in the Environment, *Surfaces*, 3(4), 516-566, <https://doi.org/10.3390/surfaces3040037>, 2020.
- 542 Anjilvel, S. and Asgharian, B.: A Multiple-Path Model of Particle Deposition in the Rat Lung, *Fundam. Appl. Toxicol.*, 28,
543 41-50, <https://doi.org/10.1006/faat.1995.1144>, 1995.
- 544 Barber, J. L., Berger, U., Chaemfa, C., Huber, S., Jahnke, A., Temme, C., and Jones, K. C.: Analysis of per- and polyfluorinated
545 alkyl substances in air samples from Northwest Europe, *J. Environ. Monit.*, 9, 530-541, <https://doi.org/10.1039/B701417A>,
546 2007.
- 547 [Batrach, M., Maskeri, L., Schubert, R., Ho, B., Kohout, M., Abdeljaber, M., Abuhasna, A., Kholoki, M., Psihogios, P., Razzaq,](#)
548 [T., Sawhney, S., Siddiqui, S., Xoubi, E., Cooper, A., Hatzopoulos, T., and Putonti, C.: Pseudomonas Diversity Within Urban](#)
549 [Freshwaters, *Front Microbiol.*, 10, 195, <https://doi.org/10.3389/fmicb.2019.00195>, 2019.](#)
- 550 [Baum, M. M., Kainović, A., O'Keefe, T., Pandita, R., McDonald, K., Wu, S., and Webster, P.: Characterization of structures](#)
551 [in biofilms formed by a *Pseudomonas fluorescens* isolated from soil, *BMC Microbiol.*, 9, 103, \[https://doi.org/10.1186/1471-\]\(https://doi.org/10.1186/1471-2180-9-103\)](#)
552 [2180-9-103](#), 2009.
- 553 Boyd Chelsea, D., Smith, T. J., El-Kirat-Chatel, S., Newell Peter, D., Dufrêne Yves, F., and O'Toole George, A.: Structural
554 Features of the *Pseudomonas fluorescens* Biofilm Adhesin LapA Required for LapG-Dependent Cleavage, Biofilm Formation,
555 and Cell Surface Localization, *J. Bacteriol.*, 196, 2775-2788, <https://doi.org/10.1128/jb.01629-14>, 2014.
- 556 Cai, W., Navarro, D. A., Du, J., Ying, G., Yang, B., McLaughlin, M. J., and Kookana, R. S.: Increasing ionic strength and
557 valency of cations enhance sorption through hydrophobic interactions of PFAS with soil surfaces, *Sci. Total Environ.*, 817,
558 152975, <https://doi.org/10.1016/j.scitotenv.2022.152975>, 2022.
- 559 Cheong, W. J. and Carr, P. W.: The Surface Tension of Mixtures of Methanol, Acetonitrile, Tetrahydrofuran, Isopropanol,
560 Tertiary Butanol and Dimethyl-Sulfoxide with Water at °C, *J. Liq. Chromatogr.*, 10, 561-581,
561 <https://doi.org/10.1080/01483918708069009>, 1987.
- 562 Charlton, S. G. V., Jana, S., and Chen, J.: Yielding behaviour of chemically treated *Pseudomonas fluorescens* biofilms,
563 *Biofilm*, 8, 100209, <https://doi.org/10.1016/j.biofilm.2024.100209>, 2024.
- 564 Cookson, E. S. and Detwiler, R. L.: Global patterns and temporal trends of perfluoroalkyl substances in municipal wastewater:
565 A meta-analysis, *Water Res.*, 221, 118784, <https://doi.org/10.1016/j.watres.2022.118784>, 2022.

566 Dai, M., Yan, N., and Brusseau, M. L.: Potential impact of bacteria on the transport of PFAS in porous media, *Water Res.*,
567 243, 120350, <https://doi.org/10.1016/j.watres.2023.120350>, 2023.

568 Després, V., Huffman, J. A., Burrows, S. M., Hoose, C., Safatov, A., Buryak, G., Fröhlich-Nowoisky, J., Elbert, W., Andreae,
569 M., Pöschl, U., and Jaenicke, R.: Primary biological aerosol particles in the atmosphere: a review, *Tellus B*, 64, 15598,
570 <https://doi.org/10.3402/tellusb.v64i0.15598>, 2012.

571 Dreyer, A., Kirchgeorg, T., Weinberg, I., and Matthias, V.: Particle-size distribution of airborne poly- and perfluorinated alkyl
572 substances, *Chemosphere*, 129, 142-149, <https://doi.org/10.1016/j.chemosphere.2014.06.069>, 2015.

573 Engvall, A. C., Krejci, R., Ström, J., Treffeisen, R., Scheele, R., Hermansen, O., and Paatero, J.: Changes in aerosol properties
574 during spring-summer period in the Arctic troposphere, *Atmos. Chem. Phys.*, 8, 445-462, [https://doi.org/10.5194/acp-8-445-](https://doi.org/10.5194/acp-8-445-2008)
575 2008, 2008.

576 Ellis, D. A., Martin, J. W., De Silva, A. O., Mabury, S. A., Hurley, M. D., Sulbaek Andersen, M. P., and Wallington, T. J.:
577 Degradation of Fluorotelomer Alcohols: A Likely Atmospheric Source of Perfluorinated Carboxylic Acids, *Environ. Sci.*
578 *Technol.*, 38, 3316-3321, <https://doi.org/10.1021/es049860w>, 2004.

579 Ervens, B. and Amato, P.: The global impact of bacterial processes on carbon mass, *Atmos. Chem. Phys.*, 20, 1777-1794,
580 <https://doi.org/10.5194/acp-20-1777-2020>, 2020.

581 Estillore, A. D., Trueblood, J. V., and Grassian, V. H.: Atmospheric chemistry of bioaerosols: heterogeneous and multiphase
582 reactions with atmospheric oxidants and other trace gases, *Chem. Sci.*, 7, 6604-6616, <https://doi.org/10.1039/C6SC02353C>,
583 2016.

584 Evich, M. G., Davis, M. J. B., McCord, J. P., Acrey, B., Awkerman, J. A., Knappe, D. R. U., Lindstrom, A. B., Speth, T. F.,
585 Tebes-Stevens, C., Strynar, M. J., Wang, Z., Weber, E. J., Henderson, W. M., and Washington, J. W.: Per- and polyfluoroalkyl
586 substances in the environment, *Science*, 375, eabg9065, <https://doi.org/10.1126/science.abg9065>, 2022.

587 Farmer, D. K., Boedicker, E. K., and DeBolt, H. M.: Dry Deposition of Atmospheric Aerosols: Approaches, Observations,
588 and Mechanisms, *Annu. Rev. Phys. Chem.*, 72, 375-397, <https://doi.org/10.1146/annurev-physchem-090519-034936>, 2021.

589 Fathollahi, A. and Coupe, S. J.: Effect of environmental and nutritional conditions on the formation of single and mixed-
590 species biofilms and their efficiency in cadmium removal, *Chemosphere*, 283, 131152,
591 <https://doi.org/10.1016/j.chemosphere.2021.131152>, 2021.

592 Faust, J. A.: PFAS on atmospheric aerosol particles: a review, *Environ. Sci.: Processes Impacts*, 25, 133-150,
593 <https://doi.org/10.1039/D2EM00002D>, 2023.

594 Finlayson-Pitts, B. J. and Pitts, J.N.: *Chemistry of the Upper and Lower Atmosphere: Theory, Experiments, and Applications*,
595 Academic Press, 298–299, San Diego, CA, 2000.

596 Folorunsho, O., Bogush, A., and Kourtchev, I.: Investigation of Per- and Polyfluoroalkyl Substances (PFAS) Adsorption onto
597 the Medium Size Quartz Gravel, *Environ. Contam. Causes Solutions.*, 1, 4, <https://doi.org/10.53941/eccs.2025.100004>, 2025.

598 Fröhlich-Nowoisky, J., Kampf, C. J., Weber, B., Huffman, J. A., Pöhlker, C., Andreae, M. O., Lang-Yona, N., Burrows, S.
599 M., Gunthe, S. S., Elbert, W., Su, H., Hoor, P., Thines, E., Hoffmann, T., Després, V. R., and Pöschl, U.: Bioaerosols in the
600 Earth system: Climate, health, and ecosystem interactions, *Atmos. Res.*, 182, 346-376,
601 <https://doi.org/10.1016/j.atmosres.2016.07.018>, 2016.

602 Gatta, E., Abd El, E., Brunoldi, M., Irfan, M., Isolabella, T., Massabò, D., Parodi, F., Prati, P., Vernocchi, V., and Mazzei, F.:
603 Viability studies of bacterial strains exposed to nitrogen oxides and light in controlled atmospheric conditions, *Sci. Rep.*, 15,
604 10320, <https://doi.org/10.1038/s41598-025-94898-y>, 2025.

605 Ge, H., Yamazaki, E., Yamashita, N., Taniyasu, S., Ogata, A., and Furuuchi, M.: Particle size specific distribution of perfluoro
606 alkyl substances in atmospheric particulate matter in Asian cities, *Environ. Sci.: Processes Impacts.*, 19, 549-560,
607 <https://doi.org/10.1039/C6EM00564K>, 2017.

608 Glüge, J., Scheringer, M., Cousins, I. T., DeWitt, J. C., Goldenman, G., Herzke, D., Lohmann, R., Ng, C. A., Trier, X., and
609 Wang, Z.: An overview of the uses of per- and polyfluoroalkyl substances (PFAS), *Environ. Sci.: Processes Impacts.*, 22,
610 2345-2373, <https://doi.org/10.1039/D0EM00291G>, 2020.

611 Guo, M., Lyu, Y., Xu, T., Yao, B., Song, W., Li, M., Yang, X., Cheng, T., and Li, X.: Particle size distribution and respiratory
612 deposition estimates of airborne perfluoroalkyl acids during the haze period in the megacity of Shanghai, *Environ. Pollut.*,
613 234, 9-19, <https://doi.org/10.1016/j.envpol.2017.10.128>, 2018.

614 Guo, B., Saleem, H., and Brusseau, M. L.: Predicting Interfacial Tension and Adsorption at Fluid–Fluid Interfaces for Mixtures
615 of PFAS and/or Hydrocarbon Surfactants, *Environ. Sci. Technol.*, 57, 8044-8052, <https://doi.org/10.1021/acs.est.2c08601>,
616 2023.

617 Harada, K., Nakanishi, S., Sasaki, K., Furuyama, K., Nakayama, S., Saito, N., Yamakawa, K., and Koizumi, A.: Particle Size
618 Distribution and Respiratory Deposition Estimates of Airborne Perfluorooctanoate and Perfluorooctanesulfonate in Kyoto
619 Area, Japan, *Bull. Environ. Contam. Toxicol.*, 76, 306-310, <https://doi.org/10.1007/s00128-006-0922-1>, 2006.

620 Hong, S., Kim, M.-W., and Jang, J.: Physical collection and viability of airborne bacteria collected under electrostatic field
621 with different sampling media and protocols towards rapid detection, *Sci. Rep.*, 11, 14598, <https://doi.org/10.1038/s41598-021-94033-7>, 2021.

622
623 Johansson, J. H., Salter, M. E., Acosta Navarro, J. C., Leck, C., Nilsson, E. D., and Cousins, I. T.: Global transport of
624 perfluoroalkyl acids via sea spray aerosol, *Environ. Sci.: Processes Impacts.*, 21, 635-649,
625 <https://doi.org/10.1039/C8EM00525G>, 2019.

626 Key, B. D., Howell, R. D., and Criddle, C. S.: Defluorination of Organofluorine Sulfur Compounds by *Pseudomonas* Sp. Strain
627 D2, *Environ. Sci. Technol.*, 32, 2283-2287, <https://doi.org/10.1021/es9800129>, 1998.

628 Klevan, C., Van Allen, O., Xia, S., Mukai, K., Gomes, A., Caines, S., Woodcock, M. J., and Pennell, K. D.: Evaluation of co-
629 foaming agents for enhanced removal of per-and polyfluoroalkyl substances (PFAS) by foam fractionation, *J. Hazard. Mater.*,
630 494, 138423, <https://doi.org/10.1016/j.jhazmat.2025.138423>, 2025.

631 Kourtehev, I., McGillen, M. R., Wenger, J., and Donahue, N. M.: Rethinking environmental boundaries for contaminants of
632 emerging concern, *Atmos. Environ.*, 361, 121492, <https://doi.org/10.1016/j.atmosenv.2025.121492>, 2025.

633 Kourtehev, I., Hellebust, S., Heffernan, E., Wenger, J., Towers, S., Diapouli, E., and Eleftheriadis, K.: A new on-line SPE LC-
634 HRMS method for the analysis of Perfluoroalkyl and Polyfluoroalkyl Substances (PFAS) in PM2.5 and its application for
635 screening atmospheric particulates from Dublin and Enniscorthy, Ireland, *Sci. Total Environ.*, 835, 155496,
636 <https://doi.org/10.1016/j.scitotenv.2022.155496>, 2022.

637 Kourtehev, I., Sebben, B. G., Brill, S., Barbosa, C. G. G., Weber, B., Ferreira, R. R., D'Oliveira, F. A. F., Dias-Junior, C. Q.,
638 Popoola, O. A. M., Williams, J., Pöhlker, C., and Godoi, R. H. M.: Occurrence of a “forever chemical” in the atmosphere
639 above pristine Amazon Forest, *Sci. Total Environ.*, 944, 173918, <https://doi.org/10.1016/j.scitotenv.2024.173918>, 2024.

640 Kutsuna, S., Hori, H., Sonoda, T., Iwakami, T., and Wakisaka, A.: Preferential solvation of perfluorooctanoic acid (PFOA) by
641 methanol in methanol–water mixtures: A potential overestimation of the dissociation constant of PFOA using a Yasuda–
642 Shedlovsky plot, *Atmos. Environ.*, 49, 411-414, <https://doi.org/10.1016/j.atmosenv.2011.12.009>, 2012.

643 Leung, S. C. E., Wanninayake, D., Chen, D., Nguyen, N.-T., and Li, Q.: Physicochemical properties and interactions of
644 perfluoroalkyl substances (PFAS) - Challenges and opportunities in sensing and remediation, *Sci. Total Environ.*, 905, 166764,
645 <https://doi.org/10.1016/j.scitotenv.2023.166764>, 2023.

646 Li, J., Zhou, L., Zhang, X., Xu, C., Dong, L., and Yao, M.: Bioaerosol emissions and detection of airborne antibiotic resistance
647 genes from a wastewater treatment plant, *Atmos. Environ.*, 124, 404-412, <https://doi.org/10.1016/j.atmosenv.2015.06.030>,
648 2016.

649 Lin, H., Lao, J.-Y., Wang, Q., Ruan, Y., He, Y., Lee, P. K. H., Leung, K. M. Y., and Lam, P. K. S.: Per- and polyfluoroalkyl
650 substances in the atmosphere of waste management infrastructures: Uncovering secondary fluorotelomer alcohols, particle
651 size distribution, and human inhalation exposure, *Environ. Int.*, 167, 107434, <https://doi.org/10.1016/j.envint.2022.107434>,
652 2022.

653 Luczkiewicz, A., Kotlarska, E., Artichowicz, W., Tarasewicz, K., and Fudala-Ksiazek, S.: Antimicrobial resistance of
654 *Pseudomonas* spp. isolated from wastewater and wastewater-impacted marine coastal zone, *Environ. Sci. Pollut. Res.*, 22,
655 19823-19834, <https://doi.org/10.1007/s11356-015-5098-y>, 2015.

656 Lyu, Y., Wang, B., Du, X., Guo, B., and Brusseau, M. L.: Air-water interfacial adsorption of C4-C10 perfluorocarboxylic
657 acids during transport in unsaturated porous media, *Sci. Total Environ.*, 831, 154905,
658 <https://doi.org/10.1016/j.scitotenv.2022.154905>, 2022.

659 [Mancini, M., Gioia, V., Simonetti, F., Frugis, A., and Cinti, S.: Evaluation of pure PFAS decrease in controlled settings. *ACS*
660 *Meas Sci Au.*, 3\(6\):444-451. <https://doi.org/10.1021/acsmasuresciau.3c00027>, 2023.](https://doi.org/10.1021/acsmasuresciau.3c00027)

661

662 Massabò, D., Danelli, S. G., Brotto, P., Comite, A., Costa, C., Di Cesare, A., Doussin, J. F., Ferraro, F., Formenti, P., Gatta,
663 E., Negretti, L., Oliva, M., Parodi, F., Vezzulli, L., and Prati, P.: ChAMBRé: a new atmospheric simulation chamber for aerosol
664 modelling and bio-aerosol research, *Atmos. Meas. Tech.*, 11, 5885-5900, <https://doi.org/10.5194/amt-11-5885-2018>, 2018.

665 Pandamkulangara Kizhakkethil, J. and Kourtchev, I.: Aerosolisation of new generation perfluoroalkyl ether carboxylic and
666 sulfonic acids from aeration of contaminated aqueous solutions, *Atmos. Environ.*, 352, 121218,
667 <https://doi.org/10.1016/j.atmosenv.2025.121218>, 2025.

668 Pandamkulangara Kizhakkethil, J., Shi, Z., Bogush, A., and Kourtchev, I.: Aerosolisation of per- and polyfluoroalkyl
669 substances (PFAS) during aeration of contaminated aqueous solutions, *Atmos. Environ.*, 334, 120716,
670 <https://doi.org/10.1016/j.atmosenv.2024.120716>, 2024.

671 Pandamkulangara Kizhakkethil, J., Shi, Z., Bogush, A., and Kourtchev, I.: Measurement report: Per- and polyfluoroalkyl
672 substances (PFAS) in particulate matter (PM10) from activated sludge aeration, *Atmos. Chem. Phys.*, 25, 5947-5958,
673 <https://doi.org/10.5194/acp-25-5947-2025>, 2025.

674 Park, D., Kim, Y. H., Woo Park, C., Hwang, J., and Kim, Y. J.: New bio-aerosol collector using a micromachined virtual
675 impactor, *J Aerosol Sci.*, 40, 415-422, <https://doi.org/10.1016/J.JAEROSCI.2008.12.007>, 2009.

676 Patel, R., Saab, L. E., Brahana, P. J., Valsaraj, K. T., and Bharti, B.: Interfacial Activity and Surface pKa of Perfluoroalkyl
677 Carboxylic Acids (PFCAs), *Langmuir*, 40, 3651-3658, <https://doi.org/10.1021/acs.langmuir.3c03398>, 2024.

678 Poopedi, E., Pierneef, R., Singh, T., and Gomba, A.: Opportunistic bacterial pathogens in bioaerosols emitted at municipal
679 wastewater treatment plants, South Africa, *Sci. Rep.*, 15, 10318, <https://doi.org/10.1038/s41598-025-95484-y>, 2025.

680 Pope III, C. A. and Dockery, D. W.: Health Effects of Fine Particulate Air Pollution: Lines that Connect, *Air Waste Manage.*
681 *Assoc. J.*, 56, 709-742, <https://doi.org/10.1080/10473289.2006.10464485>, 2006.

682 Reth, M., Berger, U., Broman, D., Cousins, I. T., Nilsson, E. D., and McLachlan, M. S.: Water-to-air transfer of perfluorinated
683 carboxylates and sulfonates in a sea spray simulator, *Environ. Chem.*, 8, 381-388, <https://doi.org/10.1071/EN11007>, 2011.

684 Romakkaniemi, S., Kokkola, H., Smith, J. N., Prisle, N. L., Schwier, A. N., McNeill, V. F., and Laaksonen, A.: Partitioning
685 of semivolatile surface-active compounds between bulk, surface and gas phase, *Geophys. Res. Lett.*, 38,
686 <https://doi.org/10.1029/2010GL046147>, 2011.

687 Schaefer, C. E., Culina, V., Nguyen, D., and Field, J.: Uptake of Poly- and Perfluoroalkyl Substances at the Air–Water
688 Interface, *Environ. Sci. Technol.*, 53, 12442-12448, <https://doi.org/10.1021/acs.est.9b04008>, 2019.

689 Schenker, U., Scheringer, M., MacLeod, M., Martin, J. W., Cousins, I. T., and Hungerbühler, K.: Contribution of Volatile
690 Precursor Substances to the Flux of Perfluorooctanoate to the Arctic, *Environ. Sci. Technol.*, 42, 3710-3716,
691 <https://doi.org/10.1021/es703165m>, 2008.

692 Sha, B., Johansson, J. H., Benskin, J. P., Cousins, I. T., and Salter, M. E.: Influence of Water Concentrations of Perfluoroalkyl
693 Acids (PFAAs) on Their Size-Resolved Enrichment in Nascent Sea Spray Aerosols, *Environ. Sci. Technol.*, 55, 9489-9497,
694 <https://doi.org/10.1021/acs.est.0c03804>, 2021.

695 Sha, B., Ungerovich, E., Salter, M. E., Cousins, I. T., and Johansson, J. H.: Enrichment of Perfluoroalkyl Acids on Sea Spray
696 Aerosol in Laboratory Experiments: The Role of Dissolved Organic Matter, Air Entrainment Rate and Inorganic Ion
697 Composition, *Environ. Sci. Technol. Lett.*, 11, 746-751, <https://doi.org/10.1021/acs.estlett.4c00287>, 2024.

698 Shoeib, M., Schuster, J., Rauert, C., Su, K., Smyth, S.-A., and Harner, T.: Emission of poly and perfluoroalkyl substances,
699 UV-filters and siloxanes to air from wastewater treatment plants, *Environ. Pollut.*, 218, 595-604,
700 <https://doi.org/10.1016/j.envpol.2016.07.043>, 2016.

701 Sillankorva, S., Neubauer, P., and Azeredo, J.: Isolation and characterization of a T7-like lytic phage for *Pseudomonas*
702 *fluorescens*, *BMC Biotechnol.*, 8, 80, <https://doi.org/10.1186/1472-6750-8-80>, 2008.

703 Steele, W. V., Chirico, R. D., Knipmeyer, S. E., and Nguyen, A.: Vapor Pressure, Heat Capacity, and Density along the
704 Saturation Line: Measurements for Benzenamine, Butylbenzene, sec-Butylbenzene, tert-Butylbenzene, 2,2-Dimethylbutanoic
705 Acid, Tridecafluoroheptanoic Acid, 2-Butyl-2-ethyl-1,3-propanediol, 2,2,4-Trimethyl-1,3-pentenediol, and 1-Chloro-2-
706 propanol, *J. Chem. Eng. Data.*, 47, 648-666, <https://doi.org/10.1021/je010083e>, 2002.

707 Stolzenburg, D., Fischer, L., Vogel, A. L., Heinritzi, M., Schervish, M., Simon, M., Wagner, A. C., Dada, L., Ahonen, L. R.,
708 Amorim, A., Baccarini, A., Bauer, P. S., Baumgartner, B., Bergen, A., Bianchi, F., Breitenlechner, M., Brilke, S., Buenrostro
709 Mazon, S., Chen, D., Dias, A., Draper, D. C., Duplissy, J., El Haddad, I., Finkenzeller, H., Frege, C., Fuchs, C., Garmash, O.,
710 Gordon, H., He, X., Helm, J., Hofbauer, V., Hoyle, C. R., Kim, C., Kirkby, J., Kontkanen, J., Kürten, A., Lampilahti, J.,
711 Lawler, M., Lehtipalo, K., Leiminger, M., Mai, H., Mathot, S., Mentler, B., Molteni, U., Nie, W., Nieminen, T., Nowak, J. B.,
712 Ojdanic, A., Onnela, A., Passananti, M., Petäjä, T., Quéléver, L. L. J., Rissanen, M. P., Sarnela, N., Schallhart, S., Tauber, C.,
713 Tomé, A., Wagner, R., Wang, M., Weitz, L., Wimmer, D., Xiao, M., Yan, C., Ye, P., Zha, Q., Baltensperger, U., Curtius, J.,
714 Dommen, J., Flagan, R. C., Kulmala, M., Smith, J. N., Worsnop, D. R., Hansel, A., Donahue, N. M., and Winkler, P. M.:

715 Rapid growth of organic aerosol nanoparticles over a wide tropospheric temperature range, *Proc. Natl. Acad. Sci. U.S.A.*, 115,
716 9122-9127, <https://doi.org/10.1073/pnas.1807604115>, 2018.

717 Torres, E.: Biosorption: A Review of the Latest Advances, *Processes*, 8, 1584 <https://doi.org/10.3390/pr8121584>, 2020.

718 Tsuda, A., Henry, F. S., and Butler, J. P.: Particle Transport and Deposition: Basic Physics of Particle Kinetics, *Compr. Physiol.*, 3, 1437-1471, <https://doi.org/10.1002/j.2040-4603.2013.tb00526.x>, 2013.

720 Ungeheuer, F., Caudillo, L., Ditas, F., Simon, M., van Pinxteren, D., Kılıç, D., Rose, D., Jacobi, S., Kürten, A., Curtius, J., and
721 Vogel, A. L.: Nucleation of jet engine oil vapours is a large source of aviation-related ultrafine particles, *Commun. Earth Environ.*, 3, 319, <https://doi.org/10.1038/s43247-022-00653-w>, 2022.

723 US EPA: Estimation Programs Interface Suite™ for Microsoft® Windows, v 4.11: [https://www.epa.gov/tsca-screening-](https://www.epa.gov/tsca-screening-tools/epi-suite-estimation-program-interface)
724 [tools/epi-suite-estimation-program-interface](https://www.epa.gov/tsca-screening-tools/epi-suite-estimation-program-interface), 2012. last access: 08th November 2025.

725 US EPA: Drinking Water Health Advisory: Hexafluoropropylene Oxide (HFPO) Dimer Acid (CASRN 13252-13-6) and HFPO
726 Dimer Acid Ammonium Salt (CASRN 62037-80-3), Also Known as “GenX Chemicals”:
727 <https://www.epa.gov/system/files/documents/2022-06/drinking-water-genx-2022.pdf>, 2022. last access: 08th November 2025.

728 Vernocchi, V., Abd El, E., Brunoldi, M., Danelli, S. G., Gatta, E., Isolabella, T., Mazzei, F., Parodi, F., Prati, P., and Massabò,
729 D.: Airborne bacteria viability and air quality: a protocol to quantitatively investigate the possible correlation by an atmospheric
730 simulation chamber, *Atmos. Meas. Tech.*, 16, 5479-5493, <https://doi.org/10.5194/amt-16-5479-2023>, 2023.

731 Wang, J. and Chen, C.: Biosorbents for heavy metals removal and their future, *Biotechnol. Adv.*, 27, 195-226,
732 <https://doi.org/10.1016/j.biotechadv.2008.11.002>, 2009.

733 Wanzek, T., Stults, J. F., Johnson, M. G., Field, J. A., and Kleber, M.: Role of Mineral–Organic Interactions in PFAS Retention
734 by AFFF-Impacted Soil, *Environ. Sci. Technol.*, 57, 5231-5242, <https://doi.org/10.1021/acs.est.2c08806>, 2023.

735 Wu, W., Jin, Y., and Carlsen, C.: Inflammatory health effects of indoor and outdoor particulate matter, *J. Allergy Clin. Immunol.*, 141, 833-844, <https://doi.org/10.1016/j.jaci.2017.12.981>, 2018.

737 Xu, P., Zhang, C., Mou, X., and Wang, X. C.: Bioaerosol in a typical municipal wastewater treatment plant: concentration,
738 size distribution, and health risk assessment, *Water Science and Technology*, 82, 1547-1559,
739 <https://doi.org/10.2166/wst.2020.416>, 2020. *Water Sci. Technol.*

740 Zhang, L. and Vet, R.: A review of current knowledge concerning size-dependent aerosol removal, *China Particology*, 4,
741 272-282, [https://doi.org/10.1016/S1672-2515\(07\)60276-0](https://doi.org/10.1016/S1672-2515(07)60276-0), 2006.